Journal of Sustainable Metallurgy (2023) 9:1512–1525
https://doi.org/10.1007/s40831-023-00743-9

RESEARCH ARTICLE

Chemical Range of Stability for Self-Dusting Ladle Furnace Slags and Destabilizing Effect of Sulfur

D. Mombelli[1] · G. Dall'Osto[1] · A. Fumagalli[1] · C. Mapelli[1]

Received: 4 April 2023 / Accepted: 27 August 2023 / Published online: 14 September 2023

Abstract

Ladle furnace slags are characterized by volumetric expansions associated with the transition of dicalcium silicate (C_2S) from β to γ phase, which generates fine dust during cooling, causing handling and storage issues that further reduce their recycling opportunities. The present work focuses on the effect of slag basicity on dusting and the role of sulfur on slag stability. Seven synthetic ladle slag precursors were made by mixing lime, magnesia, quartz and alumina in different proportions to match effective industrial compositions, increasing the binary basicity and keeping the ternary and quaternary indexes unchanged. Samples were heated to 1500 °C for 15 min and monitored during air cooling (< 5 °C/s) through thermocouples and camera to characterize the behavior, temperature, and time interval of dusting. The cooled samples were characterized chemically, mineralogically and morphologically. Starting from the chemistry of a self-stabilized slag, five additional slag precursors, characterized by increasing amounts of S, were created and analyzed using the same procedures. Experimental evidence showed the presence of three different dusting behaviors (stable, partial and complete) and stabilization of the slag once an optical basicity of 0.748 or higher was reached. In addition, mayenite was identified as the main phase capable of suppressing the β to γ transition by exerting hydrostatic pressure on C_2S. Finally, although S can stabilize the β phase when dissolved in it, after saturation it precipitates as CaS, which can react with mayenite, locally decreasing the optical basicity and allowing dusting.

Graphical Abstract

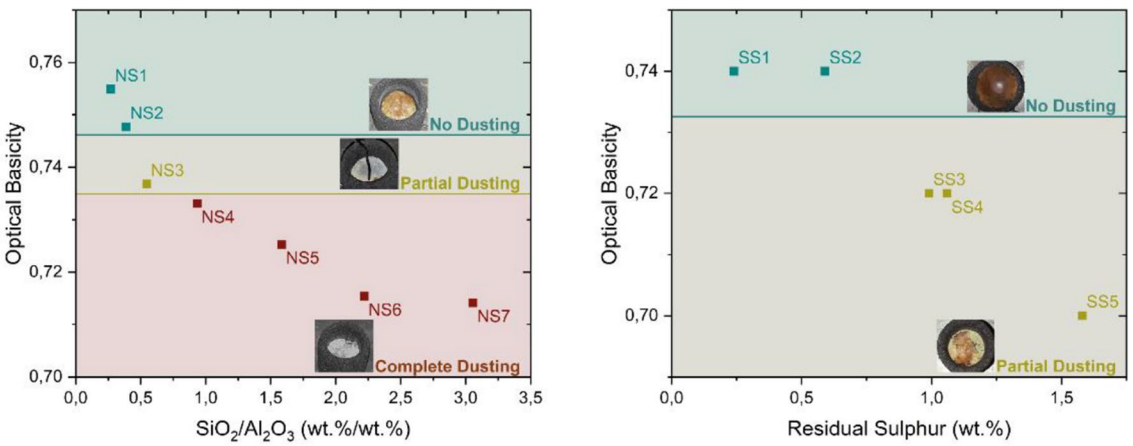

Keywords Ladle furnace slags · Dusting stabilization · Basicity · Sulfur · Dicalcium silicate

The contributing editor for this article was Sharif Jahanshahi.

Extended author information available on the last page of the article

Introduction

Ladle furnace (LF) slags are one of the key factors ruling the final steel quality at the end of secondary metallurgy processes. Their characteristic color, which has given them the additional designation of *white slag*, is due to the higher amount of lime (CaO) and magnesia (MgO) than alumina (Al_2O_3) and quartz (SiO_2) [1]. The presence of these oxides is essential for the refining step, which can be briefly summarized as deoxidation, desulfurization, removal of impurities and decarburization of the molten bath [2].

Like other slags, by-products, and wastes related to steel processes, LF slags have also been the subject of a massive research campaign for their valorization and reuse in several industrial sectors to minimize waste generation and improve sustainability, two philosophies strongly supported by the EU and steel associations [3–6]. However, despite the potential reuse of LF slags in various sectors, their actual application is very limited compared to other residues and it is mainly concentrated to the civil and road construction sector or as fluxing agents within Electric Arc Furnaces (EAFs) [2, 5, 7–9]. This discrepancy is due to the disintegration phenomenon, also known as *dusting*, that affects LF slags during the cooling and generates particles with a granulometry that can range from tens of μm up to mm [2]. As a consequence, dusting involves two main problems: the first concerns environmental safety, since the dust generated can be easily dispersed by the wind over great distances, contaminating soil, water and especially nearby work areas, whereas the second is related to the significant increase in landfill costs [10, 11].

This problem is well known in both academia and, especially, industry and is globally recognized as being caused by the allotropic transition of the dicalcium silicate ($2CaO{\cdot}SiO_2$ or C_2S) from the monoclinic β phase to the orthorhombic γ phase at about 500 °C. In particular, the volumetric expansion of about 14% is responsible for the generation of high internal stresses, leading to the subsequent disintegration of the slag even in the presence of small amounts of γ-C_2S (4%wt) [2, 12]. In a pioneering study by Parker and Ryder, published in 1942, the stability field of C_2S, adjusted on the sulfide content of the slag, was defined from CaO–MgO–SiO_2–Al_2O_3 and expressed in Eqs. (1) and (2) [13]. However, fulfilling the requirements suggested by Parker and Ryder has the main disadvantage of decreasing the metallurgical functionality of the slag at high temperature, since the low basicity would cause rapid degradation of the refractory and low Cr yield in the case of stainless steel production [14, 15].

$$CaO + 0.8MgO \leq 1.2SiO_2 + 0.39Al_2O_3 + 1.75S \quad (1)$$

$$CaO \leq 0.93SiO_2 + 0.55Al_2O_3 + 1.75S \quad (2)$$

Consequently, several studies have focused on inhibiting β to γ transformation at high temperature by adding stabilizers and additives during the cooling stage, most of which were discussed in a recently published review by Dash et al. [2]. Great attention has been paid to completely or partially displacing the CaO–MgO–SiO_2–Al_2O_3 system outside the stable C_2S region using compounds containing SiO_2 (e.g., quartz, fly ash, pearlite, etc.) or Al_2O_3 (e.g., alumina, bauxite, red mud, etc.). Indeed, their addition promotes the formation of other phases that can oppose dusting, such as merwinite ($Ca_3Mg(SiO_4)_2$) and gehlenite ($Ca_2Al(AlSiO_7)$) or mayenite ($Ca_{12}Al_{14}O_{33}$) and mellite ($Al_2[C_6(COO)_6]{\bullet}16(H_2O)$) depending on whether silica or alumina containing materials are used, respectively [10, 12, 16–22]. Similar results have been obtained with the addition of MgO and P_2O_5 compounds, the latter aiming to achieve slag chemistry similar to that of blast furnace slag, which is not affected by dusting [23, 24]. Among the additives, boron-containing materials for high temperature slag stabilization seem to be the preferred ones on an industrial scale. Depending on the specific compound (e.g., B_2O_3, H_3BO_3, $Na_2B_4O_7{\cdot}10H_2O$, $2CaO{\cdot}3B_2O_3{\cdot}5H_2O$, etc.) and the percentage introduced (0.5 to 2 wt%, or slightly higher), different effects have been observed, such as the formation of calcium borate to replace γ-C_2S or the substitution of Si^{4+} by B^{3+} ions, the latter similar to what was observed with the addition of nano or micro particles of TiO_2 by which Si^{4+} are replaced by Ti^{4+} ions [1, 10, 14, 16, 23–26].

Furthermore, because the addition of acidic compounds decreases the basicity of the slag, it was observed by both Ghorai et al. [12] and Eriksson et al. [27] that reducing the slag binary basicity index (B_2), evaluated as the CaO/SiO_2 ratio, to at least 1.7 prevents slag disintegration during cooling. Similar conclusions were reached by Zhao et al. [19] and Yang et al. [28] for slag obtained by Argon Oxygen Decarburization (AOD), also influenced by dusting, where the highest threshold value was about 1.5. An alternative to chemical stabilization is accelerated slag cooling, as commonly done in the cement industry. By dry granulation and a cooling rate of 5 °C/s, suppression of β to γ transformation was achieved for AOD slag with a B_2 of 2.2 [18, 28, 29].

Despite the great utility of studies on slag stabilization during tapping and cooling, it is of great interest to investigate how the chemistry of the slag itself affects the dusting phenomena. If this could be established, the results would make it possible to avoid the addition of stabilizers and additives and provide insight into compositions that can safely dispose of slag.

Experimental Procedure

In Fig. 1 is given the flow diagram used in the present work. Specifically, in the first part of this work, seven industrially comparable synthetic LF slag samples with increasing B_2 index and constant B_3 and B_4 indexes were produced. Each sample was monitored with *N*-type thermocouples and video cameras during cooling. The final products were analyzed mineralogically and morphologically, to evaluate the reliability of the literature stability criteria based on the slag basicity. After having identified a chemical composition able to provide self-stability and since no systematic studies have been conducted on the destabilizing effect of sulfur in conjunction with the C_2S phase transition, the five additional slag samples, with incremental S content, were produced and analyzed by the same procedures.

Non-sulfurized Synthetic Slag Production

Industrial-grade lime, quartz, alumina and magnesia were grinded, sieved below < 100 µm and mixed through a three-dimensional blender for 24 h to create seven non sulfurized synthetic LF slags, labelled NS, to obtain a quaternary oxide comparable to the industrial one. Prior to their mixing, the materials were chemically characterized to investigate the actual composition and presence of impurities through X-ray diffraction analysis (XRD), scanning electron microscopy with energy dispersive X-ray Spectrometry (SEM–EDS) and X-ray fluorescence (WD-XRF). The results are shown in the online supplementary materials (Table S1–S3, Figure S1–S4). For each slag precursor lime and magnesia were kept constant to not alter B_3 and B_4 indexes, whereas lime and alumina changed in percentage to modify the B_2 index and investigate its effect on the dusting phenomenon (Table 1).

Seven grams of each slag precursor were charged in a graphite crucible coated with zirconia and exposed to the following thermal treatment inside a lift-bottom furnace (Nabertherm LHT 02/17 LB):

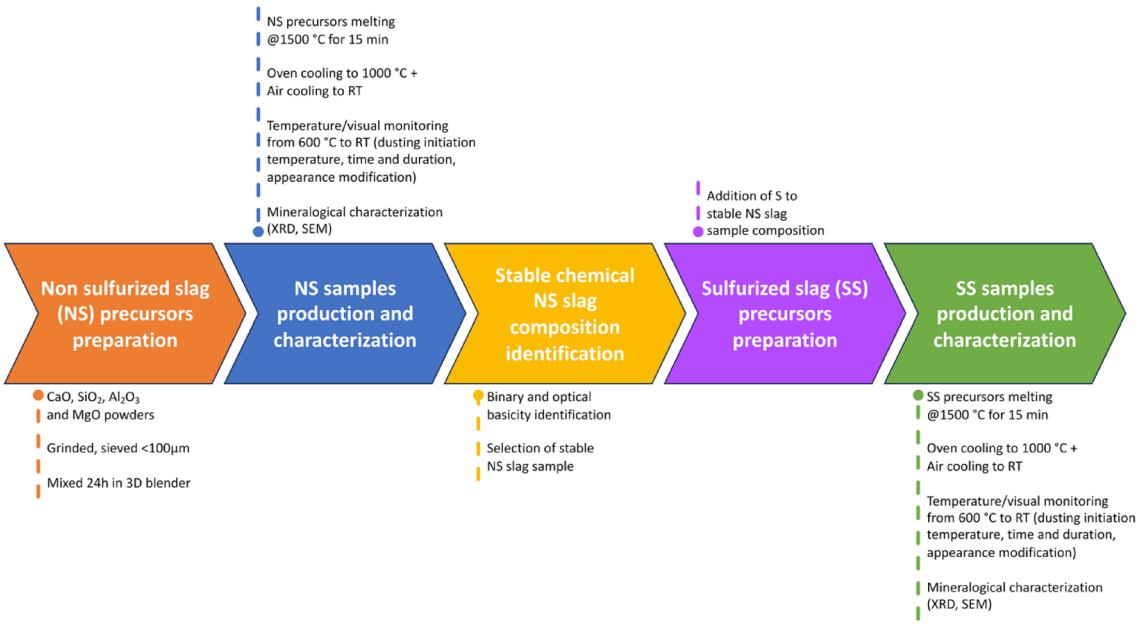

Fig. 1 Flow diagram of experimental steps

Table 1 NS slag precursor chemical composition (wt%)

	NS1	NS2	NS3	NS4	NS5	NS6	NS7
Lime	50.00	50.00	50.00	50.00	50.00	50.00	50.00
Magnesia	15.00	15.00	15.00	15.00	15.00	15.00	15.00
Alumina	30.00	25.00	22.25	17.50	12.50	10.00	7.50
Quartz	5.00	10.00	12.75	17.50	22.50	25.00	27.50

- Heating to 1500 °C (16.5 °C/min);
- Maintenance at 1500 °C for 15 min;
- Furnace cooling until 1000 °C;
- Air cooling until room temperature.

Slag Cooling Monitoring and Characterization

After the extraction of the NS slag samples from the furnace the zirconia coating was removed, and the cooling behavior filmed and time monitored. Furthermore, an *N*-type thermocouple, connected to a AT4208-Applent data logger, was placed in contact with the slag surface to record the cooling from 600 °C to room temperature. The data analysis allowed to establish the occurring, duration and number of stages of the dusting phenomenon. Specifically, the following parameters were considered:

- Temperature and time at which the first cracks due dusting occurred, if present (initiation time);
- the duration of dusting, considered as the period between the onset of dusting itself and when 50% of the surface is subjected to pulverization, since the stability of the slag is already compromised;
- any visual appearance modification of the surface during cooling.

The slag samples were chemically and morphologically characterized through a Zeiss Sigma 300 FEG-SEM equipped with Oxford Ultim Max 65 ESD probe. A Rigaku SmartLab SE diffractometer in θ–θ configuration was employed to carry out the mineralogical analysis after the milling of the samples at a granulometry lower than 100 µm. Diffracted beam was detected from 5 to 90°2θ (scan rate 5°/min, step size 0.02° and sample rotation of 30 rpm) through a 1D D/teX Ultra 250 detector. In addition, since traces of sulfur were present as impurities inside the lime (1.55 ± 0.26 wt%), Eltra elemental analyzer was used to detect the residual sulfur and carbon content.

Sulfurized Synthetic Slag Production

Five sulfurized synthetic LF slags, labeled SS, were created starting from the chemical composition of a stable NS slag sample to investigate the effect of the sulfur on the dusting phenomenon. To mitigate the evaporation during the heating, the sulfur powder was deposited on the bottom of the graphite crucible and then the stable NS slag placed above it. For each slag precursor the lime, magnesia, alumina and quartz were kept constant, whereas the amount of sulfur was increased (Table 2).

As for NS slag samples, also the SS ones have been exposed to the same thermal cycle, monitoring and characterization.

Table 2 SS Slag precursor chemical composition (wt%)

	SS1	SS2	SS3	SS4	SS5
Lime	49.29	49.27	49.28	48.95	48.60
Magnesia	14.79	14.78	14.78	14.69	14.58
Alumina	24.64	24.64	24.64	24.47	24.30
Quartz	9.86	9.86	9.86	9.79	9.72
Sulfur	1.43	1.44	1.46	2.10	2.80

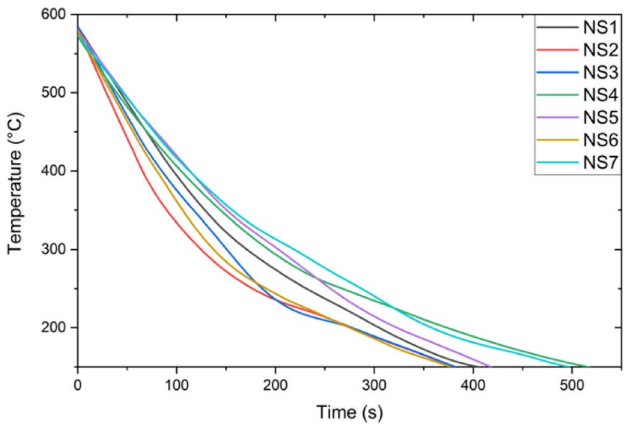

Fig. 2 Temperature–time cooling curves of NS slag samples

Results

Non Sulfurized Slag Samples

Dusting Behavior

The T-t cooling curves of the seven NS slag samples are given in Fig. 2. To compare the cooling rate of each trial the curves were fitted according to an exponential trend, which, apart slight variations relatable to the day-by-day difference of the environmental temperature, highlighted the consistency and repeatability of the cooling behaviors (Table 3).

According to literature, a rapid cooling of the slag can prevent the occurring of the dusting phenomenon, consequently a second fitting was performed in accordance with a linear trend. In the present work, all cooling rates were lower than 5 °C/s, defined as the lower threshold value for slag stability, thus all the samples were expected to experience dusting [30].

However, from the real time cooling monitoring three type of dusting were observed: no slag pulverization (Type I), partial dusting (Type II) and complete pulverization (Type III), the latter further distinguishable in continuous (Type IIIa) and stepwise (Type IIIb), respectively. The

visual appearance of the slags at the end of the cooling to room temperature are given in Fig. 3, whereas in Table 4 are summarized the main parameters and type of dusting of the NS samples.

The change in surface color appears at first glance to be associated with the type of dusting undergone by the specific sample, with the stable slags characterized by an orange surface and the dusted slags by a whitish/grayish final residue color. Additionally, comparison of the solid and dusted portions of sample NS3 confirms the hypothesis, with the former characterized by small islands of light orange color on the surface, and the latter by a white color. It is well known that slag chemistry affects the final appearance. In this specific work, samples NS1 and NS2 have the highest B_2 and optical basicity indices (meaning the lowest SiO_2/Al_2O_3 ratios), whereas NS3 sample is somewhere between the first two and the other four NS samples. Accordingly, the overall change in appearance from orange to white could be attributed to the increase in quartz, the concurrent decrease in alumina in the starting slag precursor, and the amount of sulfur retained in the synthetic slag. In fact, the increase in quartz led the final appearance to an increasingly white color, while the strongly alkaline slag (NS1 and NS2) retained a yellowish/orange color due to better sulfur binding within the lime. Finally, with the exception of dusting initiation temperature, which increases from sample NS3 to NS7, no specific trends are shown when considering dusting initiation time and duration of the whole sample. On the other hand, if a specific type of dusting is taken into consideration, samples NS5, NS6 and NS7 (Type IIIb) are characterized by

Table 3 NS slag samples cooling rates

		NS1	NS2	NS3	NS4	NS5	NS6	NS7
$T = A \bullet e^{-at}$	A [°C]	582.72	564.64	585.89	604.37	580.33	575.26	598.17
	a [s^{-1}]	0.004	0.005	0.004	0.004	0.003	0.005	0.003
$T = A - k \bullet t$	k [°C s^{-1}]	1.78	2.46	2.10	1.53	1.43	1.92	1.41

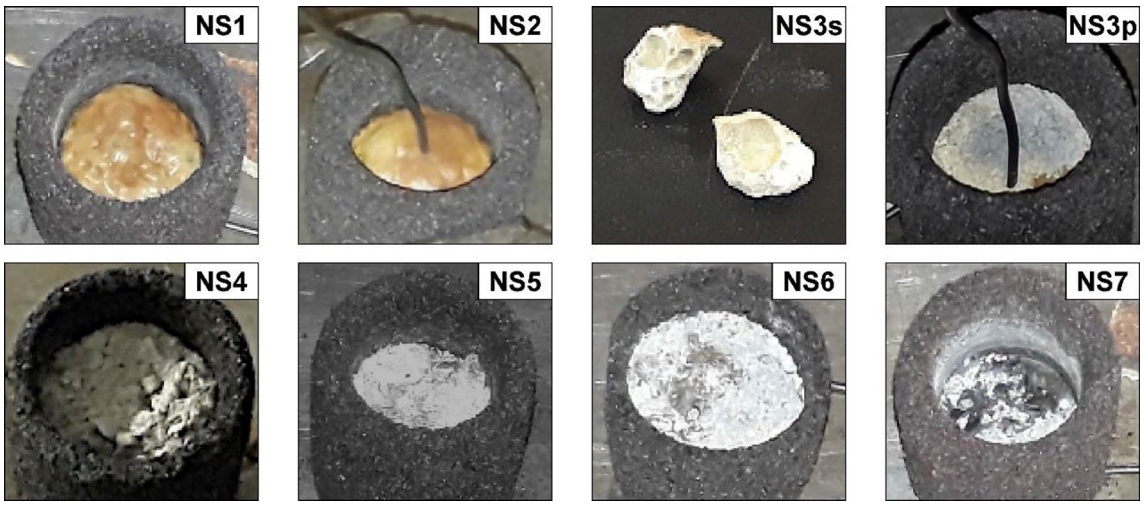

Fig. 3 Visual appearance of NS slag samples after cooling to room temperature

Table 4 NS slag samples dusting parameters

	NS1	NS2	NS3	NS4	NS5	NS6	NS7
Type	I	I	II	IIIa	IIIb	IIIb	IIIb
Dusting initiation temperature [°C]	–	–	273	285	307	308	342
Initiation time [s]	–	–	203	160	199	153	148
Dusting duration [s]	–	–	162	63	220	288	584
Surface appearance modification during cooling (from–to)	None	None	Light orange–white	Black–light grey	Black–white	Black–light grey	Black–white

an increase in dusting duration and a decrease in initiation time as a result of the increase of quartz in the slag precursor chemistry and the parallel decrease in alkalinity.

Dusting Behavior Prediction by Slag Chemistry

After cooling the chemical composition of the NS slag samples were evaluated and compared to that of other industrial and literature analyzed LF slags (Table 5). Specifically, NS1 and NS7 samples were the ones closest to the actual industrial slag chemistry, consequently the remaining samples should be considered as transition compositions.

Starting from the chemical composition the investigation on the correlation between the dusting behavior and the binary basicity index were conducted, since the slag were designed to maintain B_3 and B_4 indexes constant. Furthermore since, alumina and quartz were the only two feedstocks varying in the slag precursors chemistry they were used as additional parameter for the comparison (Fig. 4a). Although according to literature a B_2 index lower than 1.7 should be able to prevent the dusting, this was not confirmed in the present work, specifically by NS7 sample, whose B_2 index was equal to 1.66 [12, 27]. On the other hand, the increase of alumina in the slag appears to improve the resistance against the dusting. Specifically, the dusting was mitigated starting from a SiO_2/Al_2O_3 ratio lower than 0.55 (NS3) and completely suppressed at values lower than 0.39 (NS1 and NS2).

To overcome the limitation imposed by binary basicity, optical basicity, which considers all weighted contributions of the oxides contained in the slag, was used instead. (Fig. 4b). In general, high basicity (binary, ternary or optical) is considered detrimental to slag stability, since in all reported literature, dusting is observed for very alkaline slag (i.e., characterized by a high basicity value) [12, 18–20, 27, 28, 32]. However, this is not in compliance with the present work. Indeed, the NS1 and NS2 samples, which are

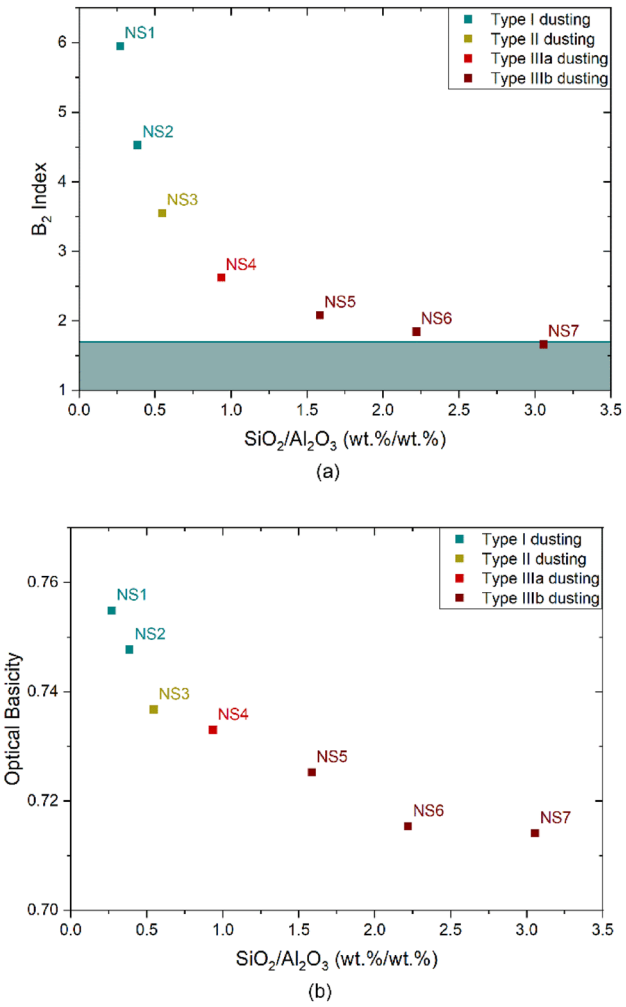

Fig. 4 **a** B_2 index and **b** optical basicity in function of SiO_2/Al_2O_3 (green area represents the B_2 values where no dusting is expected according to literature [12, 27]) (Color figure online)

Table 5 NS slag samples chemical composition after cooling (wt%)

	NS1	NS2	NS3	NS4	NS5	NS6	NS7
CaO	46.92	46.78	46.35	46.79	46.96	46.56	46.68
MgO	14.46	14.43	14.32	14.43	14.40	14.37	14.26
Al_2O_3	29.28	26.73	23.90	19.08	14.24	11.38	9.19
SiO_2	7.89	10.33	13.06	17.86	22.58	25.27	28.08
SO_3	0.30	0.22	0.08	0.22	0.44	0.37	0.38
CO_2	0.54	0.86	1.60	0.86	0.55	1.17	0.51
Others*	0.61	0.64	0.68	0.76	0.83	0.87	0.91
Industrial/literature slag closest equivalent	DOFASCO, Canada [31] Mobarakeh S.P., Iran [2, 31]				T.A. Branca [1]	T.A. Branca [1]	Tata Steel, India [12]

*oxides present in the slags in a lower content, such as Fe_2O_3, K_2O, TiO_2 and Na_2O, due to raw materials impurities

characterized by an optical basicity equal or greater than 0.74 (i.e., slag with a high of CaO/SiO_2 ratio), were not subjected to pulverization.

Mineralogical and Microscopical Slag Analysis

The evolution of the XRD spectra of the NS slag samples (Figure S5–S11), and in particular the peaks of mayenite, akermanite and both C_2S phases, is shown in Fig. 5a. The weight fraction of each mineralogical phase identified in the seven samples was evaluated by Rietveld analysis and shown in Fig. 5b**.**

Since NS1 and NS2 samples were characterized by a stable behavior upon cooling, their crystallographic phases could be considered favorable towards the slag stabilization, namely mayenite, celite, periclase and larnite. Indeed, it is worth to note the absence of the calcium olivine phase which suggests that the C_2S phase transition from β to γ has not occurred. Consequently, it is possible to assume that the high content of alumina and calcium aluminates can provide a beneficial effect on the β dicalcium silicate stability at room temperature. In particular, the quantity of mayenite found in the NS2 slag (31.3 wt%) can be assumed as the threshold above which no dusting occurs. On the other hand, NS3 and NS4 samples that can be considered as transition states due to the presence of both β and γ-C_2S, which explain the partial dusting of sample NS3 (Fig. 3). Furthermore, akermanite starts to form, whereas celite is totally absence in both samples and mayenite drastically decreases in sample NS4. The disappearing of mayenite from sample NS5 seems to confirm its stabilization effect on the β-C_2S phase. On the contrary, the increase of silica NS5, NS6 and NS7 samples had two main effects: the promotion of the dusting due to the β to γ-C_2S transition and the formation of merwinite and wollastonite.

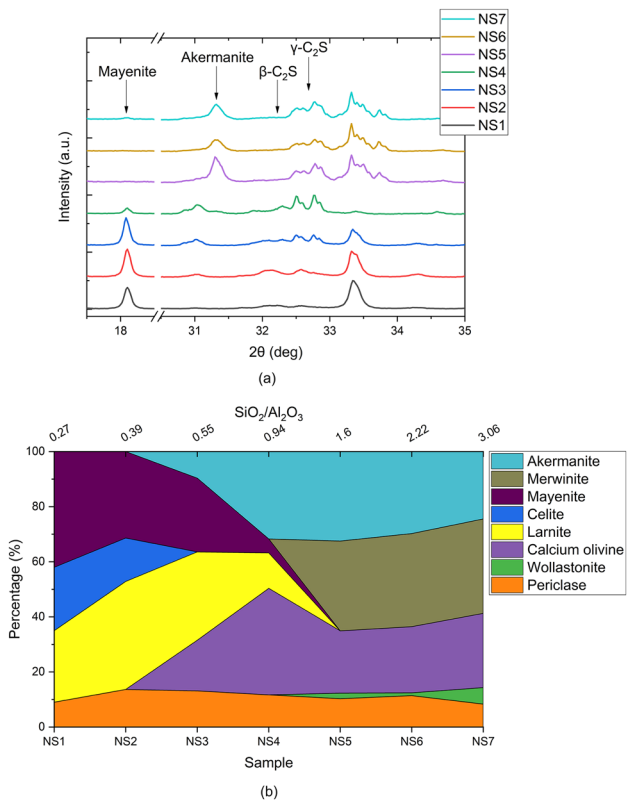

Fig. 5 **a** Main peaks of interested phases in NS slag samples and **b** Rietveld quantitative analysis results

SEM characterizations were performed on all NS samples to investigate the morphology and chemistry of the slag after cooling, the most significant SEM micrographs and corresponding EDS spectra are summarized in Fig. 6 and Table 6, respectively.

NS1 slag is denoted by a calcium aluminate matrix (spectrum A), identified as mayenite, in which ternary SiO_2-CaO-Al_2O_3 compounds (spectrum B) with a Ca/Si ratio typical of the dicalcium silicate (2:1), specifically larnite, are embedded. Particularly, larnite is the first phase that solidifies inside the liquid slag due to its dendritic morphology. Furthermore, the excess of Al detected, due to the high of alumina content of the precursor, acts as impurity in the larnite lattice and could be responsible of the stabilization of the β-C_2S form.

Both the solid and powder portions of NS3 sample have been characterized through SEM analysis to detect the possible causes of the partial dusting. The former is constituted by a calcium aluminate matrix (spectrum C), identified as mayenite, in which a dicalcium silicate phase is dispersed (spectrum D) and characterized by a fragmented appearance due to the presence of internal cracks. Although in lower extent respect to sample NS1, traces of retained Al were detected inside the latter, which may have stabilized the β-C_2S phase. Furthermore, the fragmented morphology of the dicalcium silicate suggests that during cooling it was subjected to a volumetric expansion, associable to the β to γ-C_2S transition, that was accommodated and confined by the mayenite matrix. The same phases identified in the solid fraction were observed also in the powder NS3 sample. However, it is worthy to note that while in the solid, mayenite and dicalcium silicates were in contact, in the powder the mayenite matrix (spectrum E) was separated from dicalcium silicates (spectrum F).

Finally, no significant morphological differences were observed for the NS4 and NS7 samples, consequently the characterization focused on fragmented portions to investigate the phases detrimental for the slag stability, which were identified as dicalcium silicates, specifically γ-C_2S (spectra G and H). The cracked morphology, coupled with the information gained through the XRD analysis, seems to confirm that the transition from the β to the γ phase is responsible for

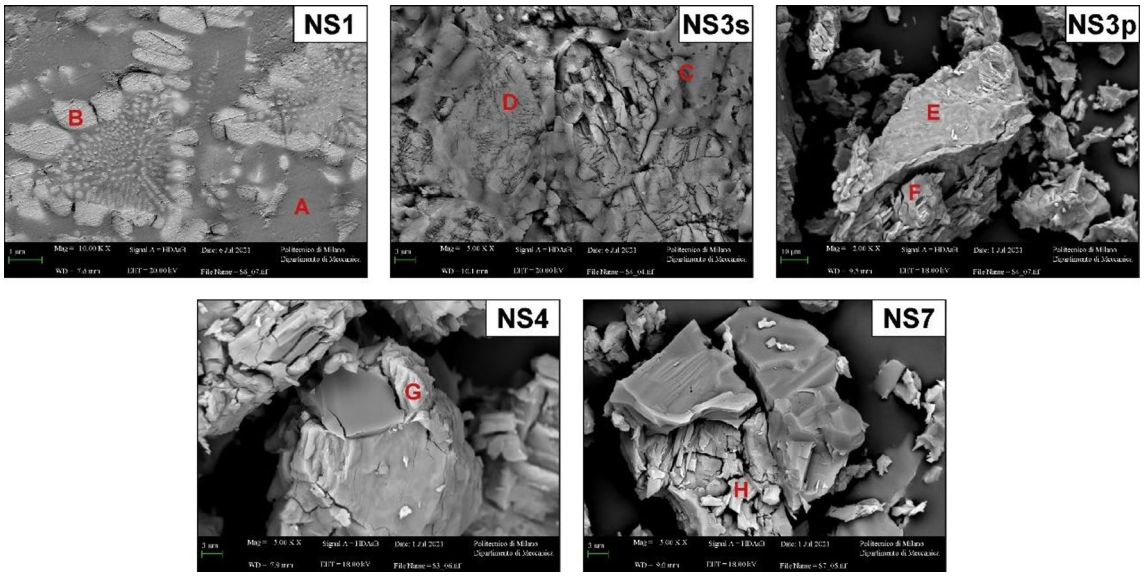

Fig. 6 Main NS slag samples SEM micrographs

Table 6 EDS spectra of NS slag samples (at%)

Sample	Spectrum	Mg	Al	Si	Ca	Phase associated
NS1	A	1.04	46.12	1.74	51.10	Mayenite
NS1	B	0.42	10.41	27.73	61.44	Larnite
NS3s	C	6.05	40.19	6.42	47.34	Mayenite
NS3s	D	0.73	2.53	30.63	66.11	β-C_2S and γ-C_2S
NS3p	E	3.86	40.53	7.83	47.78	Mayenite
NS3p	F	1.07	2.34	30.98	65.61	β-C_2S and γ-C_2S
NS4	G	6.06	1.76	34.19	57.99	γ-C_2S
NS7	H	2.08	1.88	30.77	65.28	γ-C_2S

the volumetric expansion that results in a C_2S fragmentation. Although residual Al was present in the C_2S phases, its amount is significantly less than in the NS1 samples.

Consequently, the stabilizing effect of Al seems the key for β-C_2S retention, as also reported in literature, by which a 0.5 wt% of alumina in C_2S lattice is required for the slag stability at room temperature [22]. However, in the present work the required threshold to retain the β-C_2S phase is identified at 2.97 wt% (2.53 at%). This discrepancy can be attributed to the different working conditions in the previous work (e.g. cooling rate) [22]. Besides the stabilizing effect of alumina impurities, it is worth to note that also the mayenite matrix could have a crucial role in retaining the volumetric expansion, primary thanks to its mechanical properties, as discussed later.

Sulfurized Slag Samples

Dusting Behavior and Prediction by Chemistry

NS2 slag chemistry was chosen as precursor composition to investigate the destabilizing effect of sulfur on a stable slag. The macroscopic appearance of the SS slag samples after cooling are given in Fig. 7. Similar to what was observed for the NS2 sample, which was used as the starting composition for the SS samples, the surface appearance is characterized by an even more pronounced orange/yellowish color due to the higher presence of sulfur bound to the lime.

To investigate the effect of sulfur on the slag stability during cooling, the residual sulfur and optical basicity were used as main parameters and plotted in Fig. 8 (binary basicity index is not considered since it is not subjected to any significant variations).

SS1 and SS2 slag were the only samples who do not experienced dusting probably due to their optical basicity close

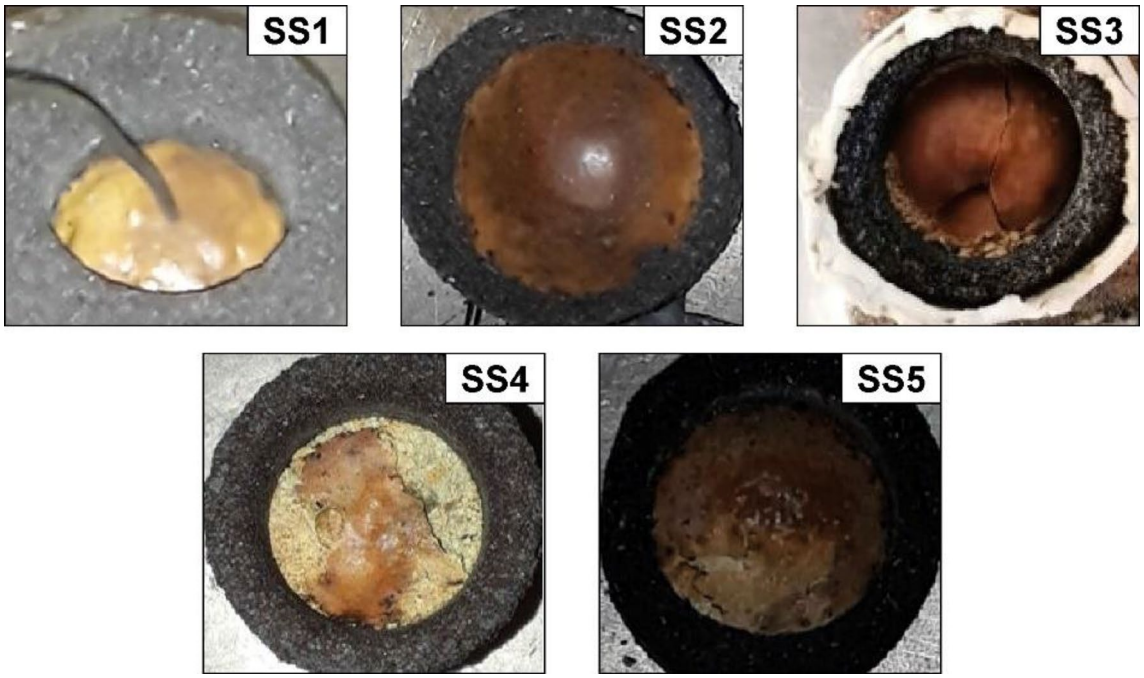

Fig. 7 Visual appearance of SS slag samples after cooling to room temperature

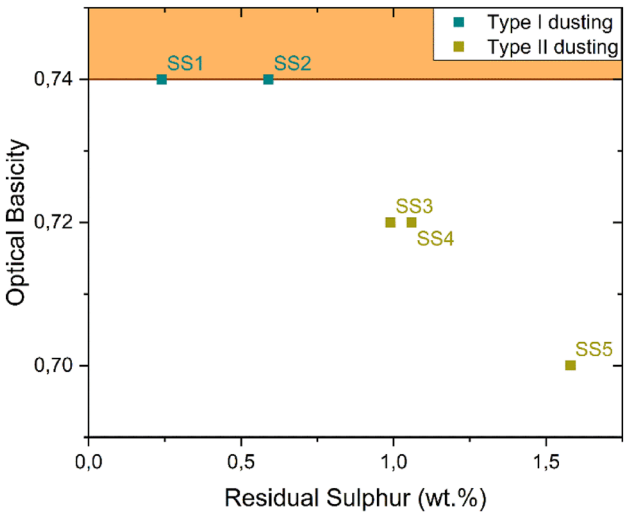

Fig. 8 Optical basicity in function of residual sulfur (orange area represents the optical basicity values where no dusting is expected)

to 0.74, value previously defined as lower stability threshold for the NS slags investigated in the present work, which confirms its effectiveness. On the other hand, the higher residual sulfur in the SS3, SS4 and SS5 samples could be responsible for the generation of calcium sulfide, due to the reaction between lime and sulfur. Thus, the CaO contribution to the optical basicity is partially removed decreasing its final value.

Table 7 SS slag samples dusting parameters

	SS1	SS2	SS3	SS4	SS5
Type	I	I	II	II	II
Dusting initiation temperature [°C]	–	–	22	147	188
Initiation time [s]	–	–	900	402	302
Dusting duration [s]	–	–	585	740	1140

In other words, the increase of sulfur content in the slag provides a detrimental effect towards the slag stability, altering the equilibrium conditions previously achieved in the NS2 slag sample.

Indeed, from the dusting parameters (Table 7) a decrease of both dusting temperature and initiation time from sample SS3 to SS5 is noted, whereas the dusting duration was subjected to the opposite effect, with lower kinetics due to the excess of sulfur.

Mineralogical and Microscopical Slag Analysis

Slag samples were characterized through XRD analysis (Figure S12–S16); in Fig. 9a is given both the evolution of C_2S phases, responsible of the dusting, and oldhamite (CaS) phase. Furthermore, the percentage of each mineralogical

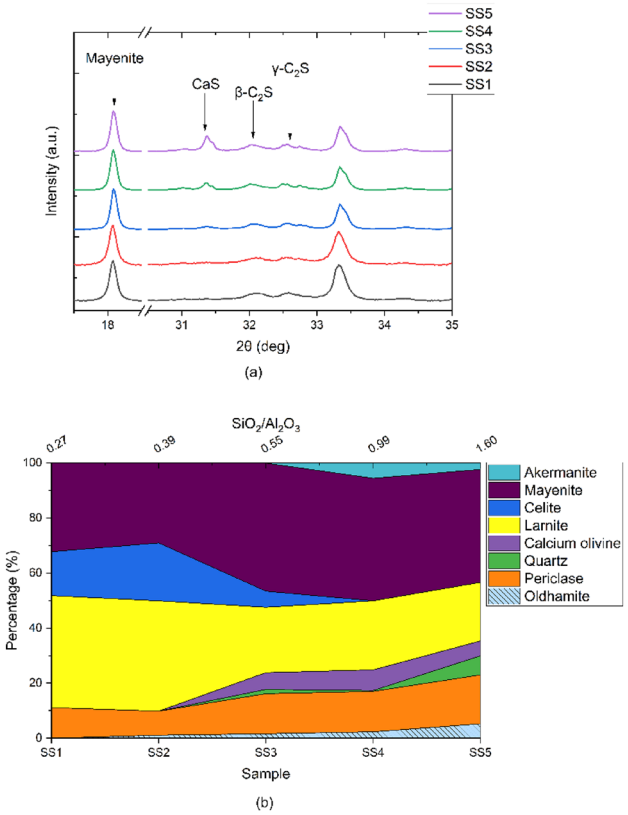

Fig. 9 **a** Main peaks of interested phases in NS slag samples and **b** Rietveld quantitative analysis results

phase in the five slag samples, evaluated through Rietveld Analysis, are given in Fig. 9b.

As for the stable NS samples, SS1 and SS2 slag samples, which do not experienced dusting, were characterized by the same main mineralogical phases, namely, mayenite, celite, periclase and larnite. Although, the higher sulfur content in the SS2 precursor led to the formation of traces of oldhamite, not detected in the SS1 one, its amount was limited and probably not able to perturbate the overall stability of the slag.

Further to the expectable increase of CaS in the remaining three SS samples, the co-presence of calcium olivine and larnite was observed, which could suggest that even though the β to γ-C_2S phase transition was incentivized by the sulfur, the transition did not occur completely. Indeed, this situation is really close to the NS3 sample, where the simultaneous presence of mayenite and β/γ-C_2S led to a type II dusting, as in the SS3, SS4 and SS5 samples.

SEM characterizations were performed on all SS samples to investigate the morphology and chemistry of the slag after cooling, the most significant SEM micrographs and corresponding EDS spectra are summarized in Fig. 10 and Table 8, respectively.

As concerns SS1 sample morphology it appears comparable to that of NS1 samples, with several corrugated structures, identified as larnite (spectrum a), embedded inside a mayenite matrix (spectrum b). More specifically,

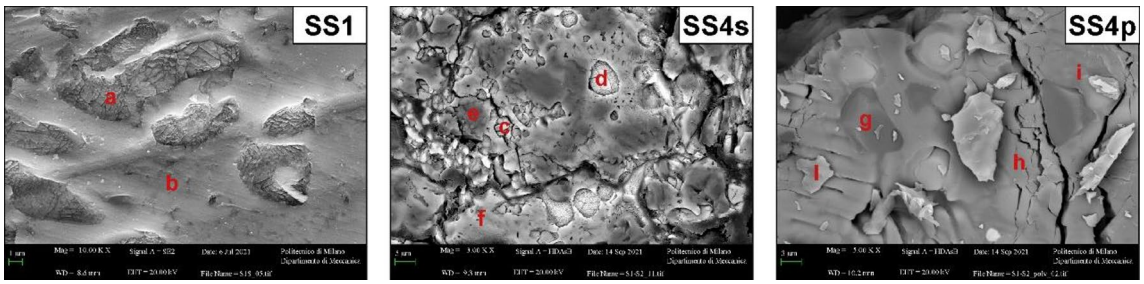

Fig. 10 Main SS slag samples SEM micrographs

Table 8 EDS spectra of SS slag samples (at.%)

Sample	Spectrum	Mg	Al	Si	Ca	S	Phase associated
SS1	a	8.82	11.58	25.64	51.80	2.16	Larnite
SS1	b	5.05	34.84	7.70	51.01	1.40	Mayenite
SS4s	c	0.32	3.24	29.22	67.22		Calcium olivine
SS4s	d		0.74		52.4	46.86	Oldhamite
SS4s	e	90.31	6.94		2.75		Periclase
SS4s	f	9.13	33.36	13.5	44.02	-	Mayenite
SS4p	g	93.79	4.18		2.03		Periclase
SS4p	h		3.96	31.1	64.91		Calcium olivine
SS4p	i				53.29	46.71	Oldhamite
SS4p	l		40.86	2.79	53.27	3.08	Mayenite

inside the former the presence of dissolved S was highlighted together with Al impurities that, as supposed for the NS samples, act as β-C_2S stabilizer. According to literature, the maximum content of sulfur that can be retained by the C_2S structure to stabilize the β phase is about 4.4 wt.%, which is nearly three times the value observed in the current SS1 sample, equal to 1.4 wt% (2.16 at%) [33]. Retained sulfur was also observed inside the mayenite matrix, which avoided the CaS precipitation. Since SS4 experienced a Type II dusting the solid and powder fractions were used as main morphologies and chemistry to describe the destabilizing effect of sulfur trough the additional use of EDS maps to better visualize the mineralogical phase distribution (Fig. 11).

The morphology of the SS4 solid fraction highlighted the presence of γ-C_2S in correspondence of the cracked surface, with a limited amount of dissolved Al (spectrum c), comparable to the value observed in the NS3s sample (Table 6). It is worthwhile to underline that no dissolved sulfur was present inside this phase, as most of it reacted with Ca to form oldhamite (spectrum d). Periclase was also observed, however due to the randomness of its position it can be considered as not relevant to the dusting (spectrum e). Finally, a quaternary $CaO–Al_2O_3–MgO–SiO_2$ compound was identified as main constituent of the solid matrix, considering the atomic ratio between Ca and Al, it is possible to label it as mayenite (spectrum f). On the other hand, the morphology of the SS4 powder fraction was comparable to that of the fractured γ-C_2S [22]. Contrary to the solid fraction, the matrix was composed mainly by dicalcium silicate due to the nearly absence of mayenite (spectra h and l). Finally, in correspondence of the cracks several agglomerates of oldhamite were observed (spectrum i).

Discussion

Cause of Slag Dusting

From the visual experimental evidence, the role of the volumetric expansion after the β to γ-C_2S phase transformation is confirmed and defined as main responsible of the dusting from the mechanical point of view. On the other hand, SEM–EDS analysis coupled with XRD spectra provided information on the main role of the stabilizer elements and mineralogical phases.

Observing the mineralogical phases NS1 and NS2 slag samples, the stability can be attributed to the high content of alumina which promotes the formation of mayenite and in minor part celite. Specifically, high contents of mayenite (higher than 31.3 wt%) exert a crucial role in the slag stabilization, since this phase acts as a matrix onto which the other phases, including the dicalcium silicate, can be dissolved. Furthermore, mayenite seems able to oppose a mechanical resistance sufficient to counteract the volumetric expansion of the β to γ-C_2S phase transformation. This hypothesis is corroborated by the observation of the NS1 and

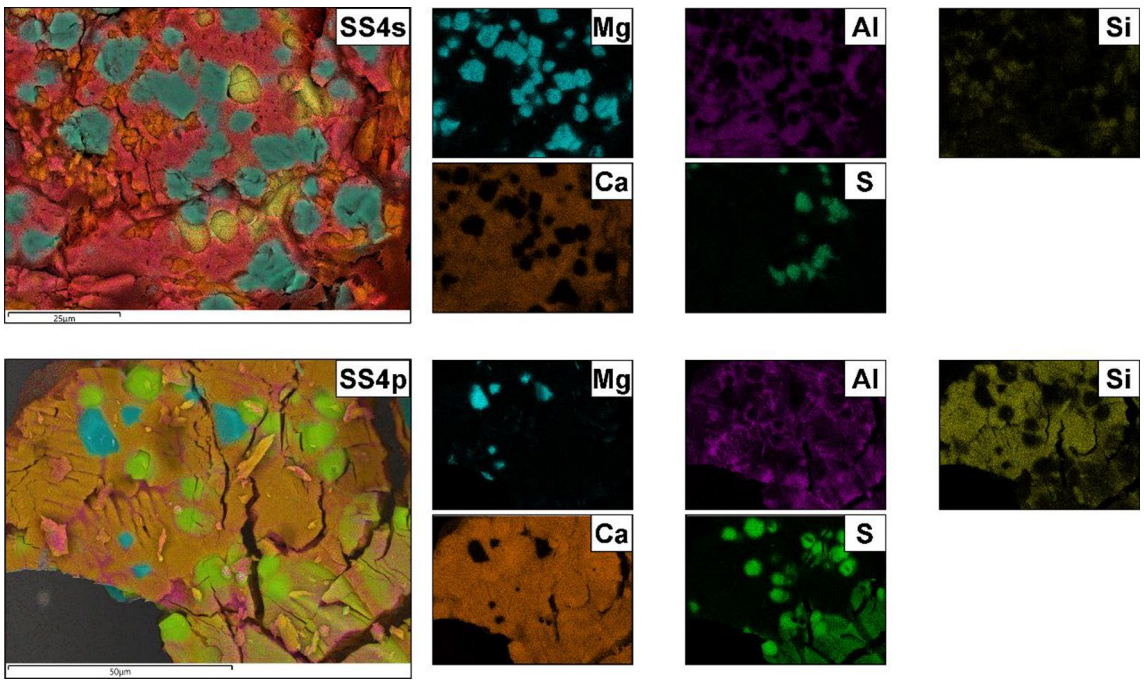

Fig. 11 SS4 solid and powder fraction EDS maps

NS2 sample, due to the exclusive presence of C_2S as larnite in the matrix. The co-presence of larnite and calcium olivine in NS3 sample is responsible of its intermediate behavior, which suggests an incomplete C_2S phase transition, probably related to the amount of mayenite present. Contrary, NS4 sample is characterized by a complete pulverization process, as expectable by the high calcium olivine content, although it still contains few mayenite and larnite, which disappear in the succeeding samples in favor of calcium olivine exclusively.

For each slag sample the presence of Al impurities inside the C_2S structures was observed by SEM–EDS analysis. According to literature the Al incorporated within the lattice of dicalcium silicate stabilizes the β-C_2S by the replacements of the silicate units and formation of vacancies [34]. In the present work, this behavior is confirmed with a lower threshold of 2.53 at%, value at which larnite is detected together with calcium olivine inside the stable portion of the NS3 slag.

However, the stabilization of larnite at room temperature by other beneficial phases cannot be excluded. As stated by the work of Chan et al. [22], the addition of alumina promotes the formation amorphous phases which mold around the C_2S particles, favoring the stabilization of β-form up to room temperature by exerting an hydrostatic constraining pressure. Probably, in the present work a thin amorphous layer has been formed between the mayenite and the dicalcium silicate stabilizing the transition of the latter. However, its amount is not enough to provide a peak in the XRD spectra. More probable, in this study, it is the mayenite itself that exerts a constrain pressure on C_2S thanks to its thermal negligible thermal expansion coefficient (10^{-6} °C^{-1}), which, during cooling, opposes to the volumetric expansion (14%) associated to the β to γ-C_2S transformation [35].

Finally, it is also worth considering the variation of SiO_2 and Al_2O_3 activities depending on the specific composition of NS slags to explain the disappearance of calcium aluminate phases in favor of calcium magnesium silicon phases. According to the literature, increasing the SiO_2 content in the slag on the one hand decreases the activity values of CaO and MgO and on the other hand increases that of Al_2O_3 [36–40]. As a result, from sample NS1 to NS7 the formation of celite and mayenite becomes less and less spontaneous, while akermanite and merwinite become more prone to form.

Sulfur Contribution to Dusting

According to literature the presence of S should act as β-C_2S stabilizer by dissolution inside the larnite phase [33, 41]. However, in the present work, the experimental evidence is partly in contrast with the literature. Indeed, on one hand, the SS1 and SS2 samples maintained their stability, thanks to the S dissolution inside the larnite, and on the other hand, once exceeded the 0.99 wt% of residual sulfur (SS3, SS4 and SS5) the dusting effect occurred, with a content of dissolved sulfur limited or even null and the formation of CaS.

The thermodynamic simulations of Kang highlighted that the precipitation of oldhamite occurs only after a specific threshold, otherwise S is contained as a solute element [42]. Consequently, by comparing SEM–EDS spectra (Table 8) and considering the order of solidification of the phases involved in the dusting, it is possible to trace a history of oldhamite precipitation and its effect on the slag stability. Based on the dendritic morphology, it can be state that the first phase to solidify is C_2S, specifically larnite, whereas the last phase is mayenite, which forms the matrix. Therefore, in the SS1 slag sample, which is characterized by the lowest level of S, it first remains trapped within β-C_2S, stabilizing it, until saturation, while the excess becomes a solute element in the mayenite matrix [42]. In the SS2 sample, on the other hand, the slightly higher concentration of S is sufficient to allow the precipitation of small amounts of CaS without significantly reducing the optical basicity. In other words, the amount of available CaO is not reduced and the slag behaves similarly to NS2 sample. Thus, larnite is still present as the only C_2S phase, and dusting is not observed, unlike the SS3, SS4, and SS5 slag samples. In fact, in these last three samples, the optical basicity is reduced, indicating the decrease of at least one specific oxide (probably CaO), β to γ transition and CaS precipitation begin to occur, both to an increasing extent, and dusting is observed. As stated by Nakai and He et al. in ladle furnace slag, the precipitation of S usually occurs as an independent phase (oldhamite), which can then react with the mayenite matrix to form $11CaO{\cdot}7Al_2O_3{\cdot}CaS$ [43, 44]. It is therefore reasonable to speculate that since this new phase has been observed in the powder fraction of the SS4 sample and not in the solid portion, where the calcium aluminate appears as pure mayenite (spectra f and l of Table 8), the restraining effect of the mayenite matrix towards the C_2S volumetric expansion was hindered to a value no longer sufficient to suppress it, thus allowing partial dusting. In addition, the reaction between CaS and $12CaO{\cdot}7Al_2O_3$ can generate a localized decrease in available CaO and binary basicity index, which consequently shifts the chemistry of the slag from the starting stable NS2 to the next unstable NS3 slag, as previously described and confirmed by the similar type of dusting (Type II) of the SS3, SS4 and SS5 samples.

Conclusions

The possibility of defining stabilization of ladle furnace slag during tapping and cooling without the implementation of additives or stabilizing agents it is of a great helpful for the safe disposal or recycling of this type of steelmaking slag. This study has confirmed that the dusting phenomenon is due to the β-C_2S to γ-C_2S transition. Furthermore, it investigated the effect of slag chemistry, particularly S, on the

slag stability. Finally, a chemical composition range able to self-stabilize a ladle furnace slag was identified.

The slag stability during air cooling (< 5 °C/s) can be described through the following observations:

- During cooling ladles slag can behave in three different ways, namely, stable, partial dusting and complete dusting.
- Optical basicity may be considered as a more reliable and comprehensive index then binary basicity to foresee the dusting. For optical basicity values higher than 0.748, both non-sulfurized and sulfurized slag samples remained stable.
- The presence of at least 2.97 wt% Al within C_2S is able to increase the β phase stability field up to room temperature, thus stabilizing the slag.
- Mayenite acts as a crucial phase for the overall slag stability, especially for its structural role as a matrix. Its presence has been detected for an Al_2O_3 content above 17.5 wt%. However, to provide sufficient hydrostatic pressure on C_2S particles and suppress the β to γ transition, a mayenite content of at least 31.3 wt% is required. This can be reached when Al_2O_3 is higher than 25 wt%.
- Although the β-stabilizer ability of S when dissolved within C_2S, the reaction between CaS and mayenite locally decreases the amount of CaO. This locally reduce the optical basicity allowing dusting to take place, even in a previously observed stable slag. This happens for a captured S content higher than 1 wt%.

Concluding, although aluminous slags can self-stabilize themselves, since them are designed to operate deep desulfurization on the steel bath, a certain amount of stabilizers must be added during tapping and air cooling at least to dilute the S below the threshold to avoid oldhamite precipitation.

Supplementary Information The online version contains supplementary material available at https://doi.org/10.1007/s40831-023-00743-9.

Author Contributions DM: conceptualization, methodology, validation, visualization, writing—original draft; GD'O: visualization, writing original draft, review and editing, resources; AF: formal analysis, investigation, data curation; CM: supervision.

Funding Open access funding provided by Politecnico di Milano within the CRUI-CARE Agreement.

Declarations

Conflict of interest On behalf of all authors, the corresponding author states that there is no conflict of interest.

References

1. Branca TA, Colla V, Valentini R (2009) A way to reduce environmental impact of ladle furnace slag. Ironmak Steelmak 36:597–602. https://doi.org/10.1179/030192309X12492910937970
2. Dash A, Chanda P, Tripathy PK, Kumar N (2022) A review on stabilization of ladle furnace slag-powdering issue. J Sustain Metall. https://doi.org/10.1007/s40831-022-00597-7
3. Malfliet A, Pontikes Y (2018) Preface to the 5th international slag valorisation symposium: from fundamentals to applications. J Sustain Metall 4:1–2. https://doi.org/10.1007/s40831-018-0168-2
4. Pontikes Y, Malfliet A (2016) Slag valorisation as a contribution to zero-waste metallurgy. J Sustain Metall 2:1–2. https://doi.org/10.1007/s40831-016-0047-7
5. Varanasi SS, More VMR, Rao MBV et al (2019) Recycling ladle furnace slag as flux in steelmaking: a review. J Sustain Metall 5:449–462. https://doi.org/10.1007/s40831-019-00243-9
6. (2022) The EIB backs Tapojarvi with EUR 18 million
7. Du C, Gao X, Kitamura S (2019) Measures to decrease and utilize steelmaking slag. J Sustain Metall 5:141–153. https://doi.org/10.1007/s40831-018-0202-4
8. Guzzon M, Mapelli C, Memoli F, Marcozzi M (2007) Recycling of ladle slag in the EAF: improvement of the foaming behavior and decrease of the environmental impact. Rev Métallurgie 104:171–178. https://doi.org/10.1051/metal:2007144
9. Matino I, Colla V, Baragiola S (2018) Internal slags reuse in an electric steelmaking route and process sustainability: simulation of different scenarios through the EIRES monitoring tool. Waste and Biomass Valorization 9:2481–2491. https://doi.org/10.1007/s12649-018-0264-3
10. Gollapalli V, Tadivaka SR, Borra CR et al (2020) Investigation on stabilization of ladle furnace slag with different additives. J Sustain Metall 6:121–131. https://doi.org/10.1007/s40831-020-00263-w
11. Branca TA, Colla V, Algermissen D et al (2020) Reuse and recycling of by-products in the steel sector: recent achievements paving the way to circular economy and industrial symbiosis in Europe. Metals (Basel) 10:345. https://doi.org/10.3390/met10030345
12. Ghorai S, Mandal GK, Roy S et al (2017) Treatment of LF slag to prevent powdering during cooling. J Min Metall Sect B Metall 53:123–130. https://doi.org/10.2298/JMMB160226004G
13. Parker TW, Ryder JF (1942) Investigations on 'falling' blast furnace slags. J Iron Steel Inst 11:21–51
14. Pontikes Y, Jones P, Geysen D, Blanpain B (2010) Options to prevent dicalcium silicate-driven disintegration of stainless steel slags. Arch Metall Mater 55:1167–1172. https://doi.org/10.2478/v10172-010-0020-6
15. Guo M, Durinck D, Jones PT et al (2007) EAF stainless steel refining - part I: observational study on chromium recovery in

an eccentric bottom tapping furnace and a spout tapping furnace. Steel Res Int 78:117–124. https://doi.org/10.1002/srin.200705868
16. Sahoo PP, Nayak P, Ranjan R (2021) Prevention of ladle furnace slag disintegration through different slag additives. J Sustain Metall 7:115–125. https://doi.org/10.1007/s40831-020-00324-0
17. Mohamed FM, El-gawad HHA, Shalabi MEH (2018) Reduction of Egyptian El-Baharia iron Ore briquettes with bentonite as binding material by Hydrogen gas in static bed. J Sustain Metall 9:441–448
18. Sakamoto N (2001) Effects of MgO based glass addition on the dusting of stainless steel slag (development of control process of stainless steel slag dusting-3). Curr Adv Mater Process 14:939
19. Zhao H, Qi Y, Shi Y et al (2013) Mechanism and prevention of disintegration of AOD stainless steel slag. J Iron Steel Res Int 20:26–30. https://doi.org/10.1016/S1006-706X(13)60078-3
20. Sheshukov OY, Nekrasov IV, Mikheenkov MA et al (2017) Stabilization of refining slag by adjusting its phase composition and giving it the properties of mineral binders. Refract Ind Ceram 58:324–330. https://doi.org/10.1007/s11148-017-0104-1
21. Iacobescu RI, Malfliet A, Machiels L et al (2014) Stabilisation and microstructural modification of stainless steel converter slag by addition of an alumina rich by-product. Waste Biomass Valorization 5:343–353. https://doi.org/10.1007/s12649-013-9287-y
22. Chan CJ, Kriven WM, Young JF (1992) Physical stabilization of the beta gamma transformation in dicalcium silicate. J Am Ceram Soc 75:1621–1627. https://doi.org/10.1111/j.1151-2916.1992.tb04234.x
23. Yan P, Nie P, Huang S et al (2014) Sulphide capacity and mineralogy of BaO and B_2O_3 modified CaO–Al_2O_3 top slag. ISIJ Int 54:1570–1577. https://doi.org/10.2355/isijinternational.54.1570
24. Durinck D, Arnout S, Mertens G et al (2008) Borate distribution in stabilized stainless-steel slag. J Am Ceram Soc 91:548–554. https://doi.org/10.1111/j.1551-2916.2007.02147.x
25. Lin Y, Luo Q, Yan B et al (2020) Effect of B_2O_3 addition on mineralogical phases and leaching behavior of synthetic CaO–SiO_2–MgO–Al_2O_3–CrOx slag. J Mater Cycles Waste Manag 22:1208–1217. https://doi.org/10.1007/s10163-020-01015-4
26. Seki A, Aso Y, Okubo M et al (1986) Development of a dusting prevention stabilizer for stainless steel slag. Kawasaki Steel Tech Rep 15:16–21
27. Eriksson J, Björkman B (2004) MgO modification of slag from stainless steelmaking. In: VII international conference on molten slags, fluxes and salts. pp. 455–459
28. Qixing Y, Nedar L, Engström F, Mingzhao H (2006) Treatments of AOD slag to produce aggregates for road construction. AISTech - iron steel technol conf proc 1:573–583
29. Kriskova L, Pontikes Y, Cizer Ö, et al (2011) Effect of the chemical composition and cooling rate on mineralogy and hydraulic properties of synthetic AOD slag. In: Proc. ECerS XII, 12th Conference of the European Ceramic Society. pp. 1–4
30. Durinck D, Engström F, Arnout S et al (2008) Hot stage processing of metallurgical slags. Resour Conserv Recycl 52:1121–1131. https://doi.org/10.1016/j.resconrec.2008.07.001
31. Behera N, Raddadi A, Ahmad S, et al (2016) Use of Al-killed ladle furnace slag in Si-killed steel process to reduce lime consumption, improve slag fluidity. In: Advances in molten slags, fluxes, and salts: proceedings of the 10th international conference on molten slags, fluxes and salts 2016. Springer International Publishing, Cham, pp. 1031–1039
32. Kriskova L, Pontikes Y, Zhang F et al (2013) Valorisation of stainless steel slags as a hydraulic binder. Acta Metall Slovaca 19:176–183. https://doi.org/10.12776/ams.v19i3.159
33. Staněk T, Sulovský P (2012) Dicalcium silicate doped with sulfur. Adv Cem Res 24:233–238. https://doi.org/10.1680/adcr.11.00021
34. Cuesta A, Aranda MAG, Sanz J et al (2014) Mechanism of stabilization of dicalcium silicate solid solution with aluminium. Dalt Trans 43:2176–2182. https://doi.org/10.1039/C3DT52194J
35. Zhou H (1993) Modification of non-metallic inclusions to improve the fatigue properties of nitriding steels
36. Ohta H, Suito H (1998) Activities of SiO_2 and Al_2O_3 and activity coefficients of FetO and MnO in CaO-SiO_2-Al_2O_3-MgO slags. Metall Mater Trans B 29:119–129. https://doi.org/10.1007/s11663-998-0014-1
37. Jung I-H, Decterov SA, Pelton AD (2005) Critical thermodynamic evaluation and optimization of the CaO–MgO–SiO_2 system. J Eur Ceram Soc 25:313–333. https://doi.org/10.1016/j.jeurceramsoc.2004.02.012
38. Guo Y, Shen F, Zheng H et al (2021) Activity of MgO in CaO–SiO_2–MgO–$Al2O_3$ melts for blast furnace slag at 1873 K. ISIJ Int 61:2021–224. https://doi.org/10.2355/isijinternational.ISIJINT-2021-224
39. Wen Q, Shen F, Zheng H et al (2018) Activity of CaO in CaO–SiO_2–Al_2O_3–MgO slags. ISIJ Int 58:792–798. https://doi.org/10.2355/isijinternational.ISIJINT-2017-735
40. Hu X, Zheng H, Guo Y et al (2020) Determination of Al_2O_3 activity by reference slag method in CaO–SiO_2–Al_2O_3–MgO melts for blast furnace slag with high Al_2O_3 at 1873 K. Steel Res Int 91:1900285. https://doi.org/10.1002/srin.201900285
41. Andrade FRD, Gomes SD, Pecchio M et al (2011) Effect of sulfur on the polymorphism and reactivity of dicalcium silicate of Portland clinker. Cerâmica 57:129–135. https://doi.org/10.1590/S0366-69132011000100017
42. Kang Y-B (2021) Progress of thermodynamic modeling for sulfide dissolution in molten oxide slags: sulfide capacity and phase diagram. Metall Mater Trans B 52:2859–2882. https://doi.org/10.1007/s11663-021-02224-4
43. Nakai Y, Kikuchi N, Iwasa M et al (2009) Development of slag recycling process in hot metal desulfurization with mechanical stirring. Steel Res Int 80:727–732
44. He HY, Ni HW, Gan WG, Lin L (2009) Sulfur's existence form and sulf-phase forming mechanism in solidified refining slag. Iron Steel 44:32–35

Authors and Affiliations

D. Mombelli[1] · G. Dall'Osto[1] · A. Fumagalli[1] · C. Mapelli[1]

✉ D. Mombelli
davide.mombelli@polimi.it

[1] Dipartimento di Meccanica, Politecnico di Milano, Via La Masa 1, 20156 Milan, Italy